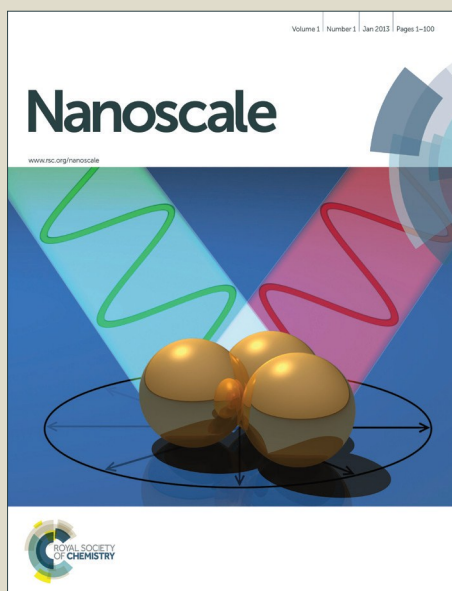


# Nanoscale

Accepted Manuscript



This is an *Accepted Manuscript*, which has been through the Royal Society of Chemistry peer review process and has been accepted for publication.

*Accepted Manuscripts* are published online shortly after acceptance, before technical editing, formatting and proof reading. Using this free service, authors can make their results available to the community, in citable form, before we publish the edited article. We will replace this *Accepted Manuscript* with the edited and formatted *Advance Article* as soon as it is available.

You can find more information about *Accepted Manuscripts* in the [Information for Authors](#).

Please note that technical editing may introduce minor changes to the text and/or graphics, which may alter content. The journal's standard [Terms & Conditions](#) and the [Ethical guidelines](#) still apply. In no event shall the Royal Society of Chemistry be held responsible for any errors or omissions in this *Accepted Manuscript* or any consequences arising from the use of any information it contains.

Biodegradable polymeric micelle-encapsulated doxorubicin  
suppresses tumor metastasis by killing circulating tumor cells

Senyi Deng<sup>1,+</sup>, Qinjie Wu<sup>1,+</sup>, Yuwei Zhao<sup>1,+</sup>, Xin Zheng<sup>1</sup>, Ni Wu<sup>1</sup>, Jing Pang<sup>2</sup>, Xuejing Li<sup>1</sup>, Cheng Bi<sup>1</sup>, Xinyu Liu<sup>1</sup>, Li Yang<sup>1</sup>, Lei Liu<sup>2</sup>, Weijun Su<sup>3</sup>, Yuquan Wei<sup>1</sup>, Changyang Gong<sup>1,\*</sup>

<sup>1</sup> *State Key Laboratory of Biotherapy/Collaborative Innovation Center of Biotherapy, West China Hospital, Sichuan University, Chengdu, 610041, P. R. China*

<sup>2</sup> *Department of Medical Oncology, Cancer Center, West China Hospital, West China Medical School, Sichuan University, Chengdu, 610041, P. R. China*

<sup>3</sup> *School of Medicine, Nankai University, Tianjin, 300071, P. R. China*

---

\* To whom correspondence should be addressed (C Gong). E-mail: [chygong14@163.com](mailto:chygong14@163.com).

+ These authors contributed equally to this work.

## Abstract

Circulating tumor cells (CTCs) play a crucial role in tumor metastasis, but rare chemotherapy policy focuses on killing CTCs. Doxorubicin (Dox) micelles which showed improved anti-metastasis activity by killing CTCs were described. Dox micelles with small particle size and high encapsulation efficiency were obtained using a pH-induced self-assembly method. Compared with free Dox, Dox micelles exhibited improved cytotoxicity, apoptosis induction effect, and cellular uptake. In addition, Dox micelles showed a sustained release behavior *in vitro*, and in transgenic zebrafish model Dox micelles showed a longer circulation time and lower extravasation from blood vessels into surrounding tissues. Anti-tumor and anti-metastasis activities of Dox micelles were investigated in transgenic zebrafish models and mouse models. In transgenic zebrafish models, Dox micelles could inhibit tumor growth and prolonged survival of tumor-bearing zebrafish. Furthermore, Dox micelles could suppress tumor metastasis by killing CTCs. Besides, improved anti-tumor and anti-metastasis activities were also confirmed in mouse tumor models. Moreover, immunofluorescent staining of tumors indicated that Dox micelles induced more apoptosis and showed fewer proliferation-positive cells. Dox micelles showed lower side effects in transgenic zebrafish and mouse models. In conclusion, Dox micelles showed stronger anti-tumor and anti-metastasis activities and lower side effects both *in vitro* and *in vivo*, which may have potential applications in cancer therapy.

**Keywords:** doxorubicin; micelle; zebrafish; self-assemble; circulating tumor cells

## 1 Introduction

As a common cancer, breast cancer shows malignant progression and poor prognosis, which is the main cause of cancer-related death among women in clinic<sup>1-4</sup>. The standard strategy in clinical treatment of breast cancer is surgery and following radiotherapy and chemotherapy. With the applications in clinical treatment of cancer, chemotherapy has been confirmed as an available and effective program<sup>5,6</sup>. However, chemotherapy in breast cancer still has to cope with some formidable problems. Breast tumor is highly invasive and metastasis<sup>7-10</sup>. Tumor cells' migrating to blood is the first step of distant metastasis. It is well known that circulating tumor cells (CTCs) play crucial roles in inducing tumor recurrence and metastasis<sup>11,12</sup>. But by now rare chemotherapy policy focuses on killing those CTCs, and failure in handling CTCs maybe the leading cause for the recurrence and metastasis in breast cancer after surgery<sup>13,14</sup>. On the other hand, most drugs used in clinical chemotherapy of breast tumor are small molecular compounds. Using those small molecular drugs brings many side effects, which would remarkably limit the intensity of chemotherapy<sup>15</sup>. Moreover, rapid elimination and widespread tissue distribution of those small molecular agents require a large dosage to keep their therapeutic concentration, and this would enhance the side effects. To face the challenge in chemotherapy of breast cancer, novel delivery strategies should be developed to improve the drug concentration at the tumor site, as well as killing the CTCs and reducing the side effects<sup>16</sup>.

Nanotechnology has shown its applied advantages in drug delivery and gained increasing attention in cancer therapy<sup>17-22</sup>. Polymeric micelle is one kind of nano-carrier, in which hydrophobic core working as drug carrier and hydrophilic shell working as an invisible cloak to the body defense system<sup>19,23</sup>. In nano-carriers based drug delivery systems (DDS), encapsulation of drug into biodegradable polymeric micelles could easily resolve the intravenous administration problem of hydrophobic drugs in chemotherapy<sup>24,25</sup>. Besides, prolonging the *in vivo* circulation time by the presence of the hydrophilic shells and their nano-size would help passively target the

tumor site under the enhanced permeability and retention (EPR) effect<sup>26</sup>. This makes possibility for gaining a therapeutic activity in a minor dose and benefiting reduced side effects while chemotherapy. Also, the prolonging of *in vivo* circulation time for drugs encapsulated in polymeric micelles increases the exposing time of circulating cells to therapeutic agents and may help to kill CTCs.

Doxorubicin (Dox) is one of the most widely used and effective anti-tumor chemotherapeutic drugs in clinic. But Dox is more considered as an inappropriate drug in clinic for its short-term and long-term cardiotoxicity<sup>27,28</sup>. In this work, Dox loaded polymeric micelles were prepared and characterized. Then, the cytotoxicity, apoptosis induction, and cellular uptake of Dox micelles were investigated in detail on 4T1 cells. By using Tg(flk1:egfp) transgenic zebrafish model, we investigated the *in vivo* extravasation of Dox micelles. In addition, the anti-tumor and anti-metastasis activities of Dox micelles were studied on 4T1 xenograft tumor model on Tg(flk1:egfp) transgenic zebrafish and subcutaneous 4T1 breast tumor model on BALB/c mice. Finally, the toxicity of Dox to blood cells and cardiac was detected on Tg(gata1:rfp) and Tg(lysz1:egfp) transgenic zebrafish models and mice model.

## 2 Materials and methods

### 2.1 Materials, cell lines, and animals

Monomethyl poly(ethylene glycol) (MPEG, Mn=2000, Fluka, USA),  $\epsilon$ -caprolactone ( $\epsilon$ -CL, Alfa Aesar, USA), stannous octoate (Sn(Oct)<sub>2</sub>, Sigma, USA), doxorubicin hydrochloride (Sigma, USA), methyl thiazolyl tetrazolium (MTT, Sigma, USA), 4',6-diamidino-2-phenylindole 2hcl (DAPI, Sigma, USA), AnnexinV-FITC/PI Detection kit (KeyGen, Nanking, China), 1-phenyl-2-thiourea (PTU, Sigma, USA), CM-DiI (Invitrogen, USA), and tricaine (Sigma, USA) were used without further purification.

4T1 mouse breast tumor cells were got from American Type Culture Collection (ATCC; Rockville, MD). Circulating tumor cells (CTCs) were isolated from blood of patients with gastric carcinoma (provided by West China Hospital). Cells were cultured in Dulbecco's modified Eagle's medium (DMEM, Gibco, USA) basic

medium supplement with 10% fetal bovine serum (FBS, Gibco, USA). The assays of cell culture and cell passage were set up as standard, and all cells were cultured at 37°C in a humidified incubator containing 5% CO<sub>2</sub>.

BALB/c mice (18 ± 2g) were used for *in vivo* anti-tumor assays. The animals were purchased from the Laboratory Animal Center of Sichuan University and maintained in an automatic raise system which offered the animals a controlled temperature of 20-22°C, relative humidity of 50-60% and 12 hours light-dark cycles. Animals were provided with standard laboratory chow and tap water *ad libitum*. All animal operations were executed according to the protocols approved by the Institutional Animal Care and Treatment Committee of Sichuan University (Chengdu, China).

## 2.2 Preparation and characterization of Dox micelles

Monomethyl poly(ethylene glycol)-poly( $\epsilon$ -caprolactone) (MPEG-PCL) diblock copolymer was synthesized by ring-opening polymerization of  $\epsilon$ -CL on MPEG using Sn(Oct)<sub>2</sub> as catalyst, which was reported in our previous contributions. The molecular weight of MPEG-PCL copolymer is 3950 (Mn, MPEG:PCL=2000:1950).

Dox was loaded into MPEG-PCL micelles through a pH-induced self-assembly method. In detail, 0.1 mL of 10× PBS (pH 7.4) was added into 0.7 mL of blank micelle solution (27.14 mg/mL), and then 0.2 mL of Dox aqueous solution (5 mg/mL) were added into the above solution dropwisely under mild stirring. One hour later, Dox micelles were prepared, and prepared Dox micelles were centrifuged through a filter with MWCO of 3 kDa to remove non-encapsulated Dox.

Particle size distribution of Dox micelles was determined by a dynamic light scattering particle size detector (Nano-ZS 90, Malvern Instruments, UK). All results were the mean of three different samples, and all data were expressed as the mean ± standard deviation (SD). Morphology of Dox micelles was observed using transmission electron microscope (TEM, H-6009IV, Hitachi, Japan).

HPLC (Waters Alliance 2695) equipped with a Waters 2998 detector was used to determine the concentration of Dox. A reversed phase C18 column (4.6 × 250 mm, 5  $\mu$ m, Inertsil/WondaSil, Japan) was used for chromatographic separation.

Encapsulation efficiency (EE) and drug loading (DL) of Dox micelles were calculated according to equations (1) and (2).

$$DL = \text{Drug}/(\text{Copolymer} + \text{Drug}) \times 100\% \quad (1)$$

$$EE = \text{Experimental drug loading}/\text{Theoretical drug loading} \times 100\% \quad (2)$$

### 2.3 Cytotoxicity and apoptosis induction of Dox micelles

Cytotoxicity of MPEG-PCL copolymer, Dox micelles and free Dox was tested on 4T1 cells. 4T1 cells were plated in 96-well plate, and after grown for 24 hours, the cells were exposed to a series of Dox micelles, free Dox, or MPEG-PCL copolymer, respectively. The viability of treated cells was evaluated using MTT analysis 48 hours after the drugs were added. The mean percentage of cell survival relative to that of untreated cells was estimated from the data of six individual experiments.

Flow cytometric (FCM) analysis of AnnexinV-FITC/PI staining by a flow cytometer (BD FCASCalibur™ Flow Cytometer, BD, USA) was employed to investigate the apoptosis induction effect of Dox micelles. 4T1 cells cultured in 6-well plates were treated with Dox micelles (100 ng/mL), free Dox (100 ng/mL), or blank micelles, respectively. Medium without treatment reagents were added as control. Cells were then stained using FITC-conjugated AnnexinV/PI staining as per the manufacturer's instructions. Both early apoptotic (Annexin V-positive, PI-negative) and late apoptotic (Annexin V-positive and PI-positive) cells were included in cell death determinations.

### 2.4 Cellular uptake of Dox micelles

Cellular uptake of Dox micelles was evaluated by FCM analysis and HPLC. 4T1 cells were transferred onto acid etched glass cover slips and cultured in DMEM medium (with 10% FBS). Cells were exposed to a series of serum-free medium which was containing blank micelles, free Dox or Dox micelles, respectively. Untreated cells were set up as control. After 0, 2 or 4 hours, the medium were removed and cells were washed by warm PBS (preheating at 37 °C). Then cells were washed twice with PBS and stained with DAPI. The uptake of the Dox micelles by 4T1 cells were observed and imaged by a confocal microscope. For FCM analysis, 4T1 cells were washed with PBS twice and then collected. The intracellular Dox fluorescence was analyzed by

FCM from 10,000 cells.

For quantification of cellular uptake of Dox micelles in 4T1 cells, cells were seeded on 24 well plates at a density of  $2 \times 10^5$  cells per well. After 24h incubating, medium were discarded and cells were exposed to serum-free medium containing blank micelles, free Dox, or Dox micelles, respectively. After exposed to drugs for 0, 2, or 4 hours, 4T1 cells were washed and harvested, and Dox was extracted by methanol and examined by HPLC (Waters Alliance HPLC 2695-2996, USA).

### **2.5 *In vitro* drug release study**

A modified dialysis method was employed to investigate the *in vitro* release behavior of Dox from Dox micelles. Briefly, 200  $\mu$ L of free Dox or Dox micelles were placed in dialysis bags (MWCO is 3.0 kDa). The dialysis bags were incubated in 10 mL of PBS (pre-warmed to 37 °C, pH = 7.4 or 5.0) containing Tween80 (0.5% wt) at 37 °C with gentle shaking (100 rpm). At specific time points, all the release media were removed and replaced by pre-warmed fresh release media. The released Dox samples were quantified by using HPLC. All the results were the mean of three test runs, and all data were expressed as the mean  $\pm$  SD.

### **2.6 *In vivo* drug extravasation study in transgenic zebrafish model**

Zebrafish as a permissive vertebrate model has performed a crucial role in cancer study. Tg(flk1:egfp) transgenic zebrafish line (Provided by Shuo Lin, UCLA, Los Angeles, CA) was a kind of zebrafish which endothelial cells were labeled by green fluorescent protein. For Dox have spontaneous red fluorescence, we used Tg(flk1:egfp) transgenic zebrafish model to study the *in vitro* drug extravasations of Dox micelles. Zebrafish embryos were collected, treated with 1-phenyl 2-thiourea(PTU) which could block the pigmentogenesis of fish, and then maintained at 28 °C in Holtfreter's solution. When fish developed to 48 hours post fertilization (hpf), we employed the perivitelline space microinjection method to inject the Dox micelles (1 mg/mL) or free Dox (1 mg/mL) into the circulation of fish (twenty zebrafish per group) by using a Flaming/Brown micropipette puller (PN-20, Narishige, Japan) equipped with a glass micropipette. A Zeiss Stemi 2000-C dissecting microscope (Carl Zeiss Micro-imaging Inc., Thornwood, NY) was used during the

injections. After injection, the distribution of Dox was detected under the DM600 confocal microscope system (DM6000 CS, Leica, Germany). Timelaps imaging was used to show the dynamic drug extravasation procedures of Dox micelles and free Dox.

### **2.7 Anti-tumor and anti-metastasis activities in transgenic zebrafish models**

To investigate the anti-tumor activity of Dox micelles and free Dox *in vivo*, we transplanted about 200 of 4T1 cells into the perivitelline space of 48 hpf Tg(flk1:egfp) transgenic zebrafish. Twenty-four hours after injection, fish were separated to four terms and each term has two repeated groups containing 20 fish: one group for anti-tumor activity evaluation and the other for survival rate detection. Then, fish were exposed to blank micelles (100 µg/mL), free Dox (5 µg/mL) or Dox micelles (5 µg/mL), and normal saline (NS) added in the last term as the control. The drug and fish water changed daily. The tumor in zebrafish embryos were quantified by measuring the long diameter and short diameter then imaged by a confocal microscope system (DM6000 CS, Leica, Germany) at 5 days post injection (dpi). The tumor volume was calculated using the equation  $Vol = (a \times b^2)/2$ , where vol is tumor volume,  $a$  is the length of the major axis, and  $b$  is the length of the minor axis.

CTCs have been reported in the tumor bearing patients and those cells were responsible for the distant metastasis and recurrence of tumor. In this study, we purposed to investigate the anti-metastasis effect of Dox micelles and gain primary tumor CTCs from clinical patient. The primary CTCs were labeled by red fluorescent protein by transfection with a RPF lentivirus. We injected about 100 primary CTCs into zebrafish perivitelline space at 48 hpf by a standard microinjection method, and then fish were maintained at 33°C in Holtfreter's solution (with PTU). Six hours later, 50 nL of Dox micelles (1 mg/mL), free Dox (1 mg/mL), or blank micelles were injected into the zebrafish circulation (20 zebrafish per group) respectively, and NS was used as control. We took images at 0 dpi and 5 dpi respectively and count the micro-metastasis in fish embryos at 5 dpi. All data were expressed as the mean ± SD.

### **2.8 *In vivo* mouse tumor models and treatment plan**

Anti-tumor and anti-metastasis activities of Dox micelles were also investigated

in subcutaneous 4T1 model and spontaneous pulmonary metastasis 4T1 model on BALB/c mice. According to the previous study, when the subcutaneous 4T1 tumor on mice grow to the size of  $\geq 5$  mm in diameter tumor cells would distantly metastasized to the pulmonary through circulation and induced a lot of new forming tumor nodules<sup>29,30</sup>. BALB/C mice ( $18 \pm 2$ g) were subcutaneously injected with 100  $\mu$ L of cell suspension containing  $5 \times 10^5$  4T1 cells in the right flank at day 0. Then tumor bearing mice were assigned randomly into 12 groups on day 3 when the tumors were palpable, and each group contained 6 mice, in which four groups were for the anti-tumor activity study, four groups for the survival study, and the last four groups for the anti-metastasis activity study.

For investigating the anti-tumor and life time elongation activities of Dox micelles, 5 days after transplanted, mice were began to inject intravenously every two days for two weeks (day 6 to day 18) with 100  $\mu$ L of NS (control), blank micelles, free Dox (5 mg/kg body weight) or Dox micelles (5 mg/kg body weight) respectively. In the tumor growth inhibition assay (four groups, each group contains 6 mice), tumor size was measured every three days from day 0 to sacrifice (day 30) by using calipers. Tumor volume was calculated according to the equation  $vol = (a \times b^2)/2$ , where  $vol$  is tumor volume,  $a$  is the length of the major axis, and  $b$  is the length of the minor axis. Mice in NS group began to die at day 30, and the other mice were sacrificed by cervical vertebra dislocation at day 30. After sacrificed, tumors in each group were harvested and weighted immediately. Besides, for investigated the life time extension of Dox micelles by anti-tumor activity, the survival of the tumor bearing mice (four groups, each group contain 6 mice) was observed until all mice died (at day 59).

Anti-metastasis activities study of Dox micelles in spontaneous pulmonary metastasis 4T1 model was preformed when the spontaneous 4T1 tumor grew to the size of  $\geq 5$  mm in diameter (9 days after injection). Mice were began to inject intravenously every two days for 10 days (day 9 to day 18) with 100  $\mu$ L of NS (control), blank micelles, free Dox (5 mg/kg body weight) or Dox micelles (5 mg/kg body weight), respectively. Mice were sacrificed by cervical vertebra dislocation at day 30. The lungs were weighted and the tumor nodules were counted just after

sacrificed. Then the lungs from tumor bearing mice were fixed by 4% wt paraformaldehyde overnight and sectioned to detect the pulmonary metastasis by following H&E staining.

### **2.9 Quantitative assessment of apoptosis**

Terminal deoxynucleotidyl transferase-mediated nick-end labeling (TUNEL) staining was used for cell apoptosis examination<sup>31</sup>. Tumor mass from subcutaneous 4T1 mice model were harvested, fixed in 4 wt% PFA, embedded in paraffin, and sectioned. TUNEL staining was operated by using an *in situ* cell apoptosis detection kit (DeadEnd™ Fluorometric TUNEL System, Promega, Madison, USA), and all performances were followed to the manufacturer's protocol. In this assay, four equal-sized fields of tumor tissue sections were randomly chosen and analyzed. The apoptotic index was calculated as a ratio of the apoptotic cell number to the total tumor cell number in each high-power field, and the data expressed by mean  $\pm$  SD.

### **2.10 Immunohistochemical determination of proliferation**

In this assay, the proliferation of tumor cells in each tumor was detected by Ki-67 immunofluorescence staining of paraffin embedded tumor tissue sections. The primary antibody and secondary antibody were rabbit anti-mouse monoclonal antibody Ki-67 (Cell Signalling Technology, USA) and FITC labeled goat anti-rabbit immunoglobulin (Invetrogene, USA), respectively. To quantify Ki-67 expression, the Ki-67 labeling index (Ki-67 LI) was calculated as number of Ki-67-positive cells/total number of cells counted under  $\times 400$  magnification in five randomly selected areas in each tumor sample by two independent investigators in a blinded fashion. The data expressed by mean  $\pm$  SD.

### **2.11 Evaluation of toxicity in transgenic zebrafish and mice model**

Tg(*gata1:rfp*) zebrafish model was one kind of transgenic zebrafish in which red blood cells were labeled by red fluorescent protein, and in Tg(*lysC:egfp*) transgenic zebrafish, monocytes were also labeled by green fluorescent protein (provided by Shuo Lin, UCLA, Los Angeles, CA). When fish developed to 48 hpf, fish embryos were treated with Dox micelles (5  $\mu\text{g}/\text{mL}$ ), free Dox (5  $\mu\text{g}/\text{mL}$ ), blank micelles or fish water respectively. 48 hours after treatment, the number of red blood cells or

monocytes (20 embryos in each group), and the construction of blood vessels (20 embryos in each group) were detected under the DM600 confocal microscope system (DM6000 CS, Leica, Germany).

To investigate the toxicity of Dox micelles in mice model, BALB/c mice ( $18 \pm 2$  g) were intravenously injected every two days for one week with 100  $\mu$ L of NS (control), blank micelles, free Dox (5 mg/kg body weight) or Dox micelles (5 mg/kg body weight), respectively (6 mice per group). Blood was isolated 7 days after drug injection and analysis by an automatic blood analyzer (MEK-6328K, NIHON, Japan). The data expressed by mean  $\pm$  SD. Hearts from tumor bearing mice in the tumor inhibition assay were fixed in 4 wt% PFA, embedded in paraffin, and sectioned. Then the HE staining of paraffin embedded sections detected the cardiac toxicity. The holes on the cardiac were measured in five randomly selected areas in each heart sample and the data expressed by mean  $\pm$  SD.

### 2.12 Statistical analysis

All statistical analysis was carried out under the SPSS 15.0 software (Chicago, IL, USA). Comparisons of tumor volume, tumor nodules number and lung weight were performed using one-way analysis of variance (ANOVA). Survival curves were generated based on the Kaplan-Meier method and Mann-Whitney U-tests determined the statistical significance. A *P* value  $<0.05$  on a 2-tailed test was considered statistically significant.

## 3 Results and discussion

### 3.1 Preparation and characterization of Dox micelles

Dox micelles were prepared using a pH-induced self-assembly method. As shown in Figure 1A, after centrifugation through a filter with molecular weight cutoff (MWCO) of 3 kDa, non-encapsulated Dox was removed from Dox micelles (left), whereas, all the Dox in free Dox group were removed after centrifugation (right). EE and DL of Dox micelles were  $98.03 \pm 1.22\%$  and  $4.85 \pm 0.06\%$ , respectively. Furthermore, in Figure 1B, the prepared Dox micelles had a small particle size of  $26.9 \pm 1.2$  nm with a very narrow distribution (PDI =  $0.083 \pm 0.007$ ). To investigate the

microstructure and confirm the particle of Dox micelles, TEM tests were conducted. In Figure 1C, spherical shape particles were observed, and diameter of the particles were 25-30 nm.

### 3.2 Cytotoxicity, apoptosis induction and cellular uptake of Dox micelles

As showed in Figure 2A, the viability of 4T1 cells decreased accordingly with the increasing in the concentration of the blank micelles. When the concentration of blank micelles was added up to 1000  $\mu\text{g/mL}$ , the cell viabilities of 4T1 cells were still higher than 90%. The cytotoxicity studies indicated that the micelles were biocompatible with very low cytotoxicity and it could be used as a safe drug delivery carrier. Figure 2B shows the significant inhibition of growth in 4T1 cells and the cell viability curve indicated its dose-dependent manner. The half maximal inhibitory concentration ( $\text{IC}_{50}$ ) of the Dox micelles was much lower than that of free Dox (mean 44.96 ng/mL versus 69.32 ng/mL,  $P < 0.01$ , ANOVA), which suggested the encapsulation of Dox in micelles improved the cytotoxic activity of Dox. Figure 2C showed the enhanced cytotoxicity of Dox micelles compared to free Dox 48 hours after treatment at the dose of 100 ng/mL.

We used FCM analysis to investigate the apoptosis induction of Dox micelles or free Dox in 4T1 cells by PI/Annexin V staining. As showed in Figure 2D, the percentage of total apoptotic cells was  $35.89 \pm 2.73\%$  in Dox micelles-treated 4T1 cells, versus  $25.76 \pm 4.17\%$  in free Dox-treated group ( $P < 0.001$ ),  $5.33 \pm 0.68\%$  in blank micelles-treated group ( $P < 0.001$ ), and  $3.62 \pm 0.76\%$  in normal saline (NS)-treated group ( $P < 0.001$ ). It demonstrated that Dox micelles induced more apoptotic cells than control groups *in vitro*.

To investigate the mechanism of Dox micelles in enhancing the cytotoxic activity and apoptosis induction of Dox, cellular uptake tests of the Dox micelles were performed. In Figure 3A, no red fluorescent signals could be detected in 4T1 cells in control group both at 0, 2, and 4 hours. For free Dox group, a red fluorescence was observed in 4T1 cells after 2 hours treatment and cells with stronger red fluorescence could be observed after 4 hours treatment. In the Dox micelles-treated group, Dox micelles could be uptake by 4T1 cells and showed a red fluorescence after 2 hours,

which was slightly brighter than free Dox-treated group. A stronger red fluorescent was detected after 4 h treatment. More cellular uptake of Dox in Dox micelles treated cells were also confirmed by FCM analysis, flow cytometric histograms (Figure 3B) presented that the uptake of Dox in Dox micelles treated 4T1 cells was much more as compared with free Dox treated cells after 4 hours incubation. In Figure 3C, after exposed to drug 2 hours, 0.288  $\mu\text{g}$  more Dox accumulation was detected in the Dox micelles-treated cells ( $5 \times 10^5$ ) than in cells treated with free Dox and the difference in cellular uptake was persistently enhanced over longer time (4h,  $1.559 \pm 0.106 \mu\text{g}$  versus  $0.873 \pm 0.026 \mu\text{g}$ ,  $P < 0.001$ ). These results suggest that encapsulation of Dox into polymeric micelles enhance the delivery of Dox into cells and increase the cytotoxic effect of the drug.

### 3.3 *In vitro* drug release and *in vivo* drug extravasation studies

As showed in Figure 4A and B, Dox micelles showed a much slower cumulative release rate contrasted to fast release profile in free Dox term both at pH=5.0 or pH=7.0. At the first 24 hours,  $84.9 \pm 6.44\%$  of the Dox released to the media in the free Dox term at pH=5.0, whereas only  $62.76 \pm 4.51\%$  of the Dox which encapsulated in the Dox micelles was released. When the pH value changes to 7.0,  $70.4 \pm 4.31\%$  of the Dox released to the media in 24h contrasted to only  $27.91 \pm 2.04\%$  of the encapsulated Dox released from the Dox micelles in 24h. The cumulative release rate of Dox from Dox micelles was  $86.45 \pm 4.5\%$  which is lower than the released rate in free Dox term ( $91.55 \pm 7.6\%$ ) at pH=5.0 in one week period, the bigger different cumulative release rate of Dox showed between Dox micelles term and free Dox term at pH=7.0,  $58.34 \pm 5.08\%$  versus  $87.29 \pm 3.02\%$  ( $P < 0.001$ ).

In this study, we used Tg(flk1:egfp) zebrafish to investigate the *in vivo* drug extravasations behaviors of Dox micelles and free Dox (Figure 4C). After free Dox injected to the fish, red fluorescence could be observed from the blood vessels and extravascular regions in 10 minutes, most nucleus of muscle cells in fish embryos could cover by the red fluorescence of Dox (free Dox 20min), which indicated the fast extravasation of free Dox from blood to surrounding tissues. Comparing with free Dox, Dox micelles showed a slow extravasation feature in this assay, Figure 4C

showed the dynamic extravasation behaviors of Dox micelles. 5 minutes after injection, Dox-derived red fluorescence was mainly occurred in the blood vessels and no red fluorescence signal could be observed in the surrounding tissues which suggesting that Dox was mostly located in the blood vessels. 30 minutes after injection, minor Dox could be detected in adjacent muscle cells. More muscle cells with Dox were visible at 40 min, but blood vessels were still the main distributed site of Dox in which fluorescence intensity was much stronger. 50 minutes after injection, bright red fluorescence was examined in the extravascular spaces. Figure 4D showed the location of Dox in muscle cells surrounding blood vessels. The results of this study demonstrated that encapsulation of Dox in polymeric micelles could decrease the extravasation speed of Dox from blood to neighborhood tissues, which may due to the difference of Dox and Dox micelles in molecular size. The endothelial cells, which formed blood vessels by tight cell junction, only allowed the free passages of small molecule such as Dox. Regarding Dox micelles with a relatively large diameter (about 27 nm), the passage of encapsulated Dox may be difficult and more slow, which may be helpful for minimizing the systemic toxicity and enhancing the therapeutic effect on tumors of Dox.

### **3.4 *In vivo* anti-tumor and anti-metastasis assays in Tg(flk1:egfp) zebrafish models**

Data has showed the successful inducing of a progressive tumor growth by transplanting tumor cells to the perivitelline space of zebrafish at 48 hpf<sup>32,33</sup>. After treated with drugs for five days (6 dpi), anti-tumor effects occurred in free Dox and Dox micelles group as contrasted to control and blank micelles group, and tumors in Dox micelles group were smaller than in free Dox group detected by microscope in bright view (Figure 5A). The blank micelles did not showed any anti-tumor effects and the blood vessels examinations confirmed the anti-tumor role of free Dox and Dox micelles maybe through inducing cell apoptosis but not infect tumor angiogenesis processes. Figure 5B showed the different anti-tumor effects between Dox micelles and free Dox by counting tumor volume ( $4.2 \pm 1.2 \times 10^{-3} \text{ mm}^3$  versus  $6.4 \pm 1.1 \times 10^{-3} \text{ mm}^3$ ). Furthermore, a significantly longer life span was observed in

Dox micelles-treated group (Figure 5C).

For evaluating the anti-metastasis activity of Dox micelles, we established a systemic metastasis tumor model in Tg(flk1:egfp) zebrafish by transplanting red fluorescent primary CTCs to fish circulation. As presented in Figure 6A, tumor nodules (red fluorescence) were formed at 48 hours after tumor cells were injected into the zebrafish perivitelline space. Number of tumor metastases in Dox micelles groups ( $20.2 \pm 4.2$ , Figure 6E) was less than that in free Dox ( $43.1 \pm 6.3$ ,  $P < 0.01$ ), blank micelles ( $56.1 \pm 7.7$ ,  $P < 0.01$ ), or control ( $57.8 \pm 6.9$ ,  $P < 0.01$ ) group. Figure 6B and Figure 6C showed CTCs in blood vessels and the formation of metastases by CTCs. To investigate the differences between tumor cell line with primary CTCs, we injected B16 mice melanoma cells into the circulation of 48 hpf Tg(flk1:egfp) fish embryos. As shown in Figure 6D, CTCs in blood vessel exhibited bulboid form and were smaller than B16 cells, which implied the unique characters for CTCs. Therefore, using primary CTCs to investigate anti-metastasis effect is closer to the clinic situation than using conventional tumor cell lines. Above all, these results demonstrated encapsulated Dox in Dox micelles could effectively enhance the anti-tumor and anti-metastasis activity of Dox in fish xenograft model.

### 3.5 *In vivo* anti-tumor and anti-metastasis assays in mouse models

In Figure 7A and C, Dox micelles exhibited a stronger anti-tumor activation in comparison with free Dox, while blank micelles did not showed any effect in suppressing tumor growth. Tumor weight in Dox micelles was  $0.34 \pm 0.06$  g (Figure 7B), versus  $0.63 \pm 0.07$  g in free Dox group ( $P < 0.01$ ),  $1.03 \pm 0.12$  g in blank micelles group ( $P < 0.01$ ), or  $1.05 \pm 0.19$  g in NS ( $P < 0.01$ ). Besides, Figure 7D showed the survival time in each group, a remarkably longer life span was detected in Dox micelles-treated group. The median survival time of mice in Dox micelles was 55 days, versus 48 days in free Dox group, 32 days in blank micelles group, and 37 days in NS group.

Furthermore, anti-metastasis activity of Dox micelles on spontaneous pulmonary metastasis of 4T1 breast carcinoma was studied in detail. In Figure 8A and B, mean number of tumor nodules in Dox micelles group was  $9 \pm 2$ , which was significantly

decreased compared with that in the free Dox ( $18 \pm 6$ ,  $P < 0.01$ ), blank micelles ( $47 \pm 10$ ,  $P < 0.01$ ), or NS group ( $43 \pm 12$ ,  $P < 0.01$ ). Meanwhile, weight of lungs in Dox micelles group ( $0.22 \pm 0.03$  g, Figure 8D) was significantly lower than that in free Dox ( $0.29 \pm 0.05$  g,  $P < 0.01$ ), blank micelles ( $0.41 \pm 0.08$  g,  $P < 0.01$ ), or NS ( $0.39 \pm 0.06$  g,  $P < 0.01$ ) groups. HE staining of lung slice also showed the serious metastasis in NS/blank micelles/free Dox treated group but not Dox micelles treated group (Figure 8C).

It is well known that distant metastasis of cancer cells mainly through blood vessels. Our data has showed the slow extravasations of Dox micelles from blood vessels to extravascular tissues, we presumed extending the accumulation time of Dox in circulation by encapsulating Dox in Dox micelles could efficiently kill those metastatic 4T1 tumor cells in blood vessels and increase the concentration of Dox in tumor site to increase the anti-tumor and anti-metastasis activity of Dox.

### 3.6 Determination of tumor cell proliferation

In this assay, the proliferation of tumor cells in each tumor was detected by Ki-67 immunofluorescence staining. In Figure 9A-D, weak Ki-67 special fluorescent signals were observed in the Dox micelles and free Dox treated group as contrasted with the NS and blank micelles treated group, and the Dox micelles-treated group showed a distinguished suppression in cell proliferation than the free Dox group. Figure 9E showed the Ki-67 LI, which was  $20.86 \pm 3.15\%$  in Dox micelles treated group, versus  $31.53 \pm 3.60\%$  in free Dox group ( $P < 0.01$ ),  $56.73 \pm 4.39\%$  in blank micelles group ( $P < 0.01$ ), or  $52.8 \pm 5.77\%$  in NS ( $P < 0.01$ ). No significant difference showed between NS-treated and blank micelles treated groups ( $P > 0.05$ ).

### 3.7 Assessment of tumor cell apoptosis

As shown in Figure 10A-D, more TUNEL positive cells in tumor region were observed in Dox micelles treated group compared with those in free Dox, blank micelles or NS treated group. The apoptosis index in Dox micelles treated group ( $33.73 \pm 2.70\%$ ) was significantly higher than that in free Dox ( $17.07 \pm 2.51\%$ ,  $P < 0.01$ ), blank micelles ( $6.0 \pm 1.73\%$ ,  $P < 0.01$ ), or NS ( $6.60 \pm 1.61\%$ ,  $P < 0.01$ ) groups, and no remarkable differences were detected between blank micelles and NS groups

( $P > 0.05$ ).

### 3.8 Evaluation of toxicity in transgenic zebrafish and mice model

Tg(gata1:RFP) zebrafish model was one kind of transgenic zebrafish in which red blood cells were labeled by red fluorescent protein. Monocytes were also labeled by green fluorescent protein in Tg(lysC:EGFP) zebrafish. Those fish embryos could be used for investigating the dynamic biological behaviors of blood cells *in vivo*. After treated with drugs for 48 hours (96 hpi), significantly decreasing in the number of red blood cells and monocytes were observed on fish embryos in Dox micelles and free Dox treated groups especially in free Dox treated group (Figure 11A(a,b)). In the red blood cells evaluation assays,  $26.67 \pm 7.64\%$  of fish in Dox micelles-treated group presented a decrease in red blood cells, versus  $41.67 \pm 7.64\%$  in free Dox group ( $P < 0.01$ ) and no remarkable decreasing in red blood cells was observed in NS and blank micelles group (Figure 11B).

Forty-eight hours (96 dpi) after drug was added, we count the monocytes in a standing somites of zebrafish (Figure 11C), the number of monocytes in Dox micelles was  $122 \pm 10$ , versus  $92 \pm 10$  in free Dox group ( $P < 0.01$ ),  $157 \pm 16$  in blank micelles group ( $P < 0.01$ ), or  $156 \pm 13$  in NS ( $P < 0.01$ ). No significant difference was detected between NS and blank micelles treated group ( $P > 0.05$ ). Besides, our data have also shown extending the accumulation time of Dox in circulation by Dox micelles did not destruct the blood vessels or influence the patency of blood vessels (Figure 11A(c,d)).

In mice model, mice in Dox micelles group showed a slight decrease in red blood cells and leukocytes compared with free Dox treated mice (Figure 12A and B). The average number of WBCs (white blood cells) in Dox micelles treated group was  $4.25 \pm 0.54 (\times 10^9/L)$  versus  $3.08 \pm 0.20 (\times 10^9/L)$  in free Dox group ( $P < 0.01$ ),  $8.78 \pm 0.87 (\times 10^9/L)$  in blank micelles group ( $P < 0.01$ ), or  $8.82 \pm 0.84 (\times 10^9/L)$  in NS ( $P < 0.01$ ). Besides, the average number of RBCs (red blood cells) in Dox micelles treated group was  $10.87 \pm 0.27 (\times 10^{12}/L)$  versus  $9.67 \pm 0.35 (\times 10^{12}/L)$  in free Dox group ( $P < 0.01$ ),  $11.06 \pm 0.20 (\times 10^{12}/L)$  in blank micelles group ( $P < 0.01$ ), or  $11.04 \pm 0.19 (\times 10^{12}/L)$  in NS ( $P < 0.01$ ). No significant difference was detected between NS

and blank micelles treated group ( $P>0.05$ ). The data above from transgenic zebrafish and mice model suggested encapsulating Dox in Dox micelles could reduce the toxicity of Dox to cells in circulation. In other words, enhancing the effect of Dox in anti-tumor and anti-metastasis activation by extending the accumulation time of Dox in circulation through encapsulating Dox in Dox micelles did not increase its toxicity in blood but may limit its toxicity in blood cells by reducing the toxicity in bone marrow.

Meanwhile, we compared the cardiotoxicity between Dox micelles and free Dox in BALB/c mice model. After intravenously injected every two days for two weeks with 100  $\mu$ L of NS (control), blank micelles, free Dox (5 mg/kg body weight) or Dox micelles (5 mg/kg body weight) respectively, mice in Dox micelles and free Dox all shown cardiomyopathy as contrasted to mice in NS group (Figure 12C). Degree of cardiotoxicity in Dox micelles group was slighter than that in free Dox group, because more myocardial rupture holes were observed in free Dox group. Mice in blank micelles did not presented any cardiotoxicity confirmed the safety of copolymers. All data above demonstrated encapsulating Dox in Dox micelles could reduce the toxicity of Dox *in vivo*.

#### 4 Conclusions

Dox micelles with small particle size and high EE was prepared and used for anti-tumor and anti-metastasis evaluations in transgenic zebrafish models and mouse models. Compared with free Dox, encapsulation of Dox into polymeric micelles could improve *in vitro* cytotoxicity, apoptosis induction effects, and cellular uptake. Dox micelles showed a sustained release behavior in vitro and slow extravasation behavior from blood vessels in transgenic zebrafish model. Furthermore, in xenograft transgenic zebrafish models and mouse tumor models, Dox micelles exhibited stronger anti-tumor activities than free Dox, and Dox micelles could dramatically inhibit tumor metastasis by killing CTCs. Besides, immunofluorescent assays also confirmed the improved anti-tumor and anti-metastasis activities of Dox micelles. Therefore, the Dox micelles prepared in this work exhibited enhanced anti-tumor and

anti-metastasis activities, which could serve as a potential nanomedicine for cancer therapy.

### Declaration of interest statement

The authors report no conflicts of interest. The authors alone are responsible for the content and writing of the paper.

### Acknowledgment

This work was financially supported by National Natural Science Foundation of China (NSFC81201724), Specialized Research Fund for the Doctoral Program of Higher Education (20120181120044), and Distinguished young scholars of Sichuan University (2013SCU04A16).

### References

1. J. I. Herschkowitz, W. Zhao, M. Zhang, J. Usary, G. Murrow, D. Edwards, J. Knezevic, S. B. Greene, D. Darr, M. A. Troester, S. G. Hilsenbeck, D. Medina, C. M. Perou and J. M. Rosen, *Proc. Natl. Acad. Sci. U S A*, 2012, **109**, 2778-2783.
2. R. Siegel, D. Naishadham and A. Jemal, *CA-Cancer J. Clin.*, 2013, **63**, 11-30.
3. C. I. Li, J. R. Daling and K. E. Malone, *Cancer Epidem. Biomar.*, 2005, **14**, 1008-1011.
4. A. Jemal, R. Siegel, E. Ward, T. Murray, J. Xu and M. J. Thun, *CA-Cancer J. Clin.*, 2007, **57**, 43-66.
5. R. F. Ozols, M. A. Bookman and R. C. Young, *N. Engl. J. Med.*, 2006, **354**, 1641-1643.
6. D. Elias, F. Blot, A. El Otmany, S. Antoun, P. Lasser, V. Boige, P. Rougier and M. Ducreux, *Cancer*, 2001, **92**, 71-76.
7. D. Madhavan, M. Zucknick, M. Wallwiener, K. Cuk, C. Modugno, M. Scharpf, S. Schott, J. Heil, A. Turchinovich, R. Yang, A. Benner, S. Riethdorf, A. Trumpp, C. Sohn, K. Pantel, A. Schneeweiss and B. Burwinkel, *Clin. Cancer Res.*, 2012, **18**, 5972-5982.
8. G. Sharma, S. Mirza, R. Parshad, A. Srivastava, S. Datta Gupta, P. Pandya and R. Ralhan, *Clin. Biochem.*, 2010, **43**, 373-379.
9. Y. Zhu, F. Yu, Y. Jiao, J. Feng, W. Tang, H. Yao, C. Gong, J. Chen, F. Su, Y. Zhang and E. Song, *Clin. Cancer Res.*, 2011, **17**, 7105-7115.
10. F. C. Bidard, C. Mathiot, S. Delaloge, E. Brain, S. Giachetti, P. de Cremoux, M. Marty and J. Y. Pierga, *Ann. Oncol.*, 2010, **21**, 729-733.
11. M. Yu, A. Bardia, B. S. Wittner, S. L. Stott, M. E. Smas, D. T. Ting, S. J. Isakoff, J. C. Ciciliano, M. N. Wells, A. M. Shah, K. F. Concannon, M. C. Donaldson, L. V. Sequist, E. Brachtel, D. Sgroi, J. Baselga, S. Ramaswamy, M. Toner, D. A. Haber and S. Maheswaran, *Science*, 2013, **339**, 580-584.
12. M. Yu, S. Stott, M. Toner, S. Maheswaran and D. A. Haber, *J. Cell Biol.*, 2011, **192**, 373-382.
13. M. Cristofanilli, G. T. Budd, M. J. Ellis, A. Stopeck, J. Matera, M. C. Miller, J. M. Reuben, G. V. Doyle, W. J. Allard, L. W. M. M. Terstappen and D. F. Hayes, *N. Engl. J. Med.*, 2004, **351**, 781-791.

14. M. Wallwiener, S. Riethdorf, A. D. Hartkopf, C. Modugno, J. Nees, D. Madhavan, M. R. Sprick, S. Schott, C. Domschke and I. Baccelli, *BMC Cancer*, 2014, **14**, 512.
15. D. K. Armstrong, B. Bundy, L. Wenzel, H. Q. Huang, R. Baergen, S. Lele, L. J. Copeland, J. L. Walker, R. A. Burger and G. Gynecologic Oncology, *N. Engl. J. Med.*, 2006, **354**, 34-43.
16. T. M. Allen and P. R. Cullis, *Science*, 2004, **303**, 1818-1822.
17. V. Wagner, A. Dullaart, A. K. Bock and A. Zweck, *Nat. Biotechnol.*, 2006, **24**, 1211-1217.
18. R. K. Jain and T. Stylianopoulos, *Nat. Rev. Clin. Oncol.*, 2010, **7**, 653-664.
19. B. Y. Kim, J. T. Rutka and W. C. Chan, *N. Engl. J. Med.*, 2010, **363**, 2434-2443.
20. O. C. Farokhzad, J. Cheng, B. A. Teply, I. Sherifi, S. Jon, P. W. Kantoff, J. P. Richie and R. Langer, *P. Natl. Acad. Sci. USA*, 2006, **103**, 6315-6320.
21. K. L. Hennenfent and R. Govindan, *Ann. Oncol.*, 2006, **17**, 735-749.
22. C. Gong, Y. Xie, Q. Wu, Y. Wang, S. Deng, D. Xiong, L. Liu, M. Xiang, Z. Qian and Y. Wei, *Nanoscale*, 2012, **4**, 6004-6017.
23. M. Yokoyama, *Expert Opin. Drug Del.*, 2010, **7**, 145-158.
24. X. Guo, C. Shi, G. Yang, J. Wang, Z. Cai and S. Zhou, *Chem. Mater.*, 2014, **26**, 4405-4418.
25. X. Guo, C. Shi, J. Wang, S. Di and S. Zhou, *Biomaterials*, 2013, **34**, 4544-4554.
26. J. Fang, H. Nakamura and H. Maeda, *Adv. Drug Deliver. Rev.*, 2011, **63**, 136-151.
27. S. M. Swain, F. S. Whaley and M. S. Ewer, *Cancer*, 2003, **97**, 2869-2879.
28. D. L. Hershman, R. B. McBride, A. Eisenberger, W. Y. Tsai, V. R. Grann and J. S. Jacobson, *J. Clin. Oncol.*, 2008, **26**, 3159-3165.
29. X. Huang, M. K. Wong, H. Yi, S. Watkins, A. D. Laird, S. F. Wolf and E. Gorelik, *Cancer Res.*, 2002, **62**, 5727-5735.
30. A. Ghochikyan, A. Davtyan, A. Hovakimyan, H. Davtyan, A. Poghosyan, A. Bagaev, R. I. Ataulkhanov, E. L. Nelson and M. G. Agadjanyan, *Clin. Exp. Metastas.*, 2014, **31**, 185-198.
31. Y. Gavrieli, Y. Sherman and S. A. Ben-Sasson, *J. Cell Biol.*, 1992, **119**, 493-501.
32. C. Zhao, X. Wang, Y. Zhao, Z. Li, S. Lin, Y. Wei and H. Yang, *PLoS ONE*, 2011, **6**, e21768.
33. C. Zhao, H. Yang, H. Shi, X. Wang, X. Chen, Y. Yuan, S. Lin and Y. Wei, *Carcinogenesis*, 2011, **32**, 1143-1150.

## Figure Captions

**Figure 1** Preparation and characterization of Dox micelles. A: Appearance of free Dox (right) and Dox micelles (left) after centrifugation; B: Particle size distribution of Dox micelles; C: TEM image of Dox micelles.

**Figure 2** Cytotoxicity and apoptosis induction of Dox micelles. A: Cytotoxicity evaluation of blank micelles on 4T1 breast tumor cells; B: Cytotoxicity studies of free Dox and Dox micelles on 4T1 breast tumor cells; C: Images of 4T1 cells after 48 hours drug treatment, scale bar: 100  $\mu\text{m}$ ; D: Apoptosis induction of Dox micelles and free Dox.

**Figure 3** Cellular uptakes of Dox micelles and free Dox. A: Timelaps imaging the cellular uptake of Dox micelles and free Dox on 4T1 cells, red fluorescence indicates the cellular uptake of Dox while blue fluorescence indicates the cell nuclei which is staining by DAPI. Scale bar: 20  $\mu\text{m}$ ; B: Flow cytometric histograms for the Dox micelles on 4T1 cells; C: Dox accumulation in 4T1 cell by HPLC assay.

**Figure 4** *In vitro* release behavior and *in vivo* extravasation study of Dox micelles in Tg(flkl:egfp) transgenic zebrafish model. A and B: *In vitro* release behavior of Dox micelles and free Dox at pH 5.0 and pH 7.0, respectively; C: Dynamic extravasation behaviors of Dox micelles and free Dox in Tg(flkl:egfp) transgenic zebrafish model, scale bar: 150  $\mu\text{m}$ ; D: Distribution of Dox in extravascular tissue, scale bar: 10  $\mu\text{m}$ .

**Figure 5** Anti-tumor studies of Dox micelles on Tg(flkl:egfp) transgenic zebrafish model. A: Images of anti-tumor effect in zebrafish 4T1 tumor model by Dox micelles and free Dox, scale bar: 200  $\mu\text{m}$ ; B: Tumor volume in each treatment group; C: Survival rate of zebrafish in each treatment group.

**Figure 6** Anti-metastasis studies of Dox micelles in human primary CTCs injected Tg(flkl:egfp) transgenic zebrafish model. A: images of enhanced anti-metastasis effect of Dox micelles as contrasted to free Dox in human primary CTCs injected Tg(flkl:egfp) transgenic zebrafish model, scale bar: 100  $\mu\text{m}$ ; B: Distribution of human primary CTCs in zebrafish blood vessels on 48 hpf, scale bar: 10  $\mu\text{m}$ ; C: Distribution of micro-metastases in extravascular tissue on 96 hpf, scale bar: 10  $\mu\text{m}$ ;

D: Morphologic appearance of primary CTCs and B16 cell in zebrafish blood vessel, scale bar: 5  $\mu\text{m}$ ; E: Number of micro-metastases in zebrafish extravascular tissue after 48 hours drug treatment.

**Figure 7** Dox micelles inhibit tumor growth in subcutaneous 4T1 model. A: Representative photographs of subcutaneous tumor in each treatment group; B: Tumor weight; C: Tumor volume; D: survival curve of mice in each group.

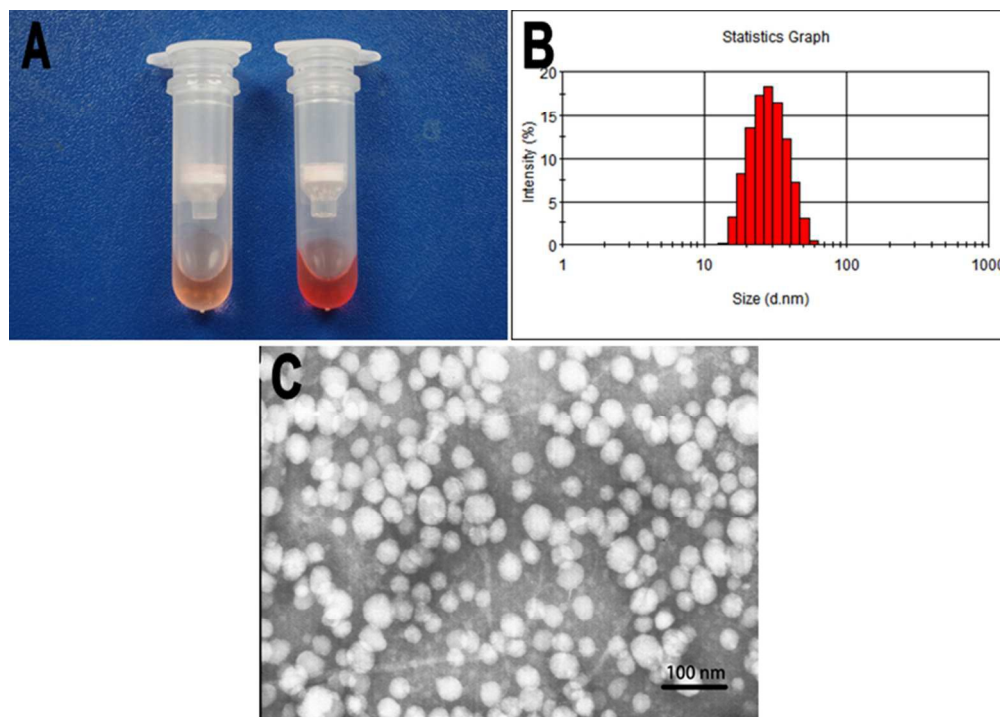
**Figure 8** Dox micelles inhibit pulmonary metastasis in spontaneous metastatic 4T1 model. A: Representative photographs of pulmonary metastases in each group; B: Number of pulmonary metastases; C: HE staining of pulmonary section, scale bar: 400  $\mu\text{m}$ ; D: Weight of lungs.

**Figure 9** Ki67 immunofluorescent staining of subcutaneous 4T1 tumor section, which suggested cell proliferation in subcutaneous 4T1 tumor. Representative Ki67 immunofluorescent images of NS (A), blank micelles (B), free Dox (C), and Dox micelles (D), and mean of Ki67 LI in each group (E).

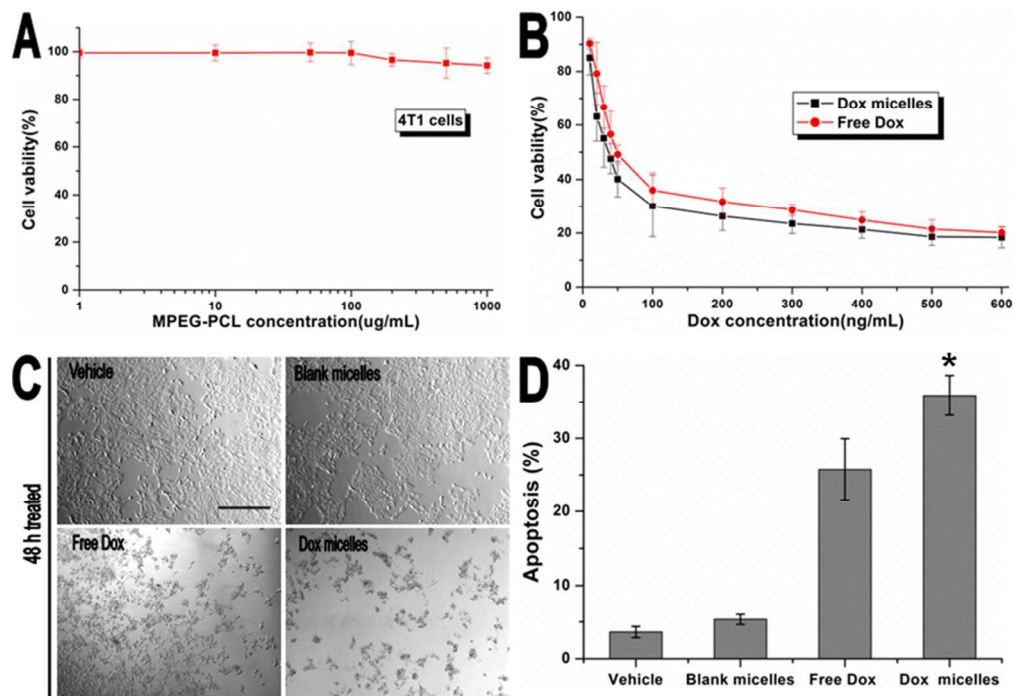
**Figure 10** TUNEL immunofluorescent staining of subcutaneous 4T1 tumor section, which suggests cell apoptosis in subcutaneous 4T1 tumor. Representative TUNEL immunofluorescent images of NS (A), blank micelles (B), free Dox (C), and Dox micelles (D), and mean of apoptosis index in each group (E).

**Figure 11** Toxicity evaluations of Dox micelles in transgenic zebrafish. A: Toxicity of Dox micelles to monocytes (a), RBCs (b) and ECs (c, d) in transgenic zebrafish model, scale bar: 100  $\mu\text{m}$ ; B: Toxicity evaluation of Dox micelles to RBCs in Tg(flk1:egfp) zebrafish; C: Monocytes number of Tg(lysC:egfp) transgenic zebrafish in each treatment group.

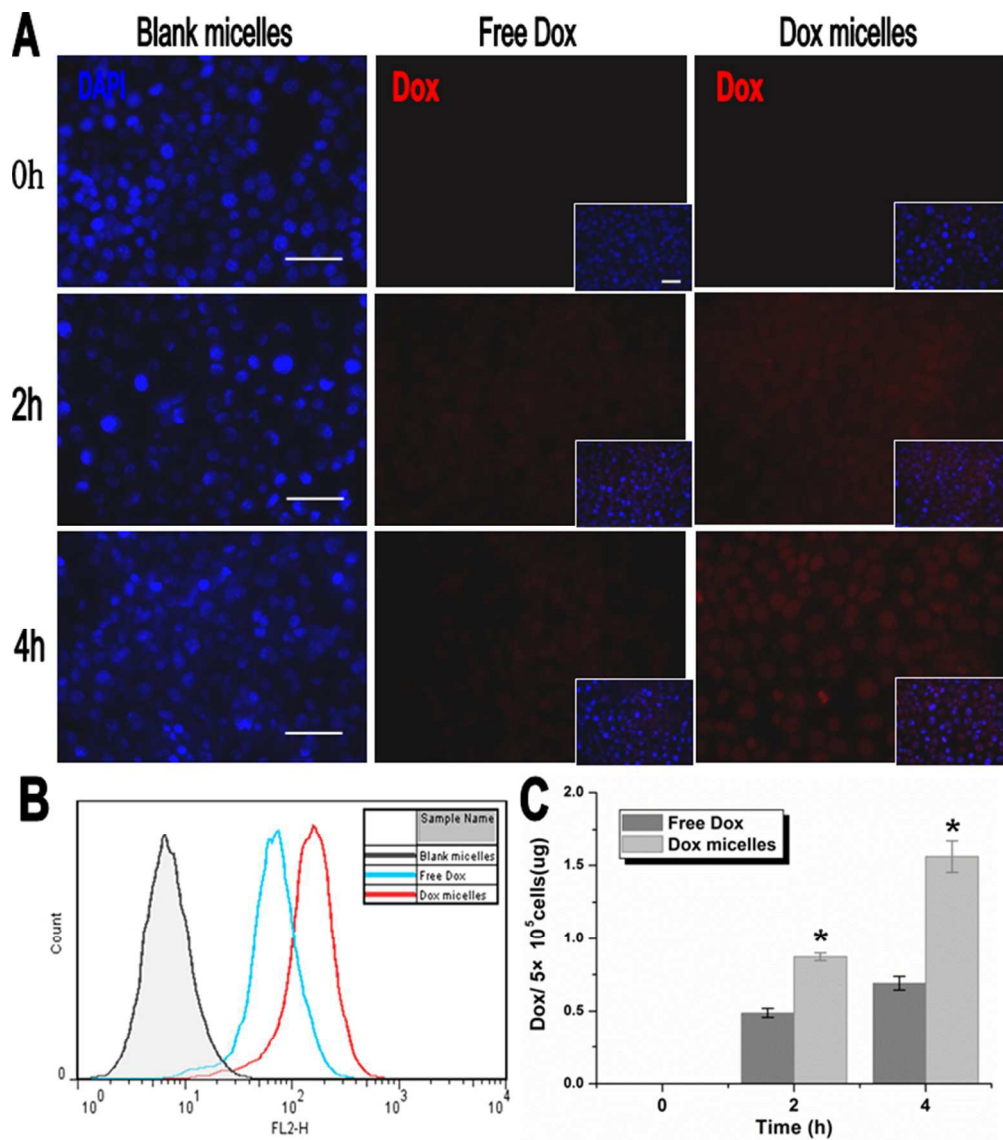
**Figure 12** Toxicity evaluations of Dox micelles in mouse model. A: WBCs counting in each group; B: RBCs counting in each group; C: Cardiotoxicity evaluation of Dox micelles in mouse model. Black arrows showed the myocardial rupture holes.



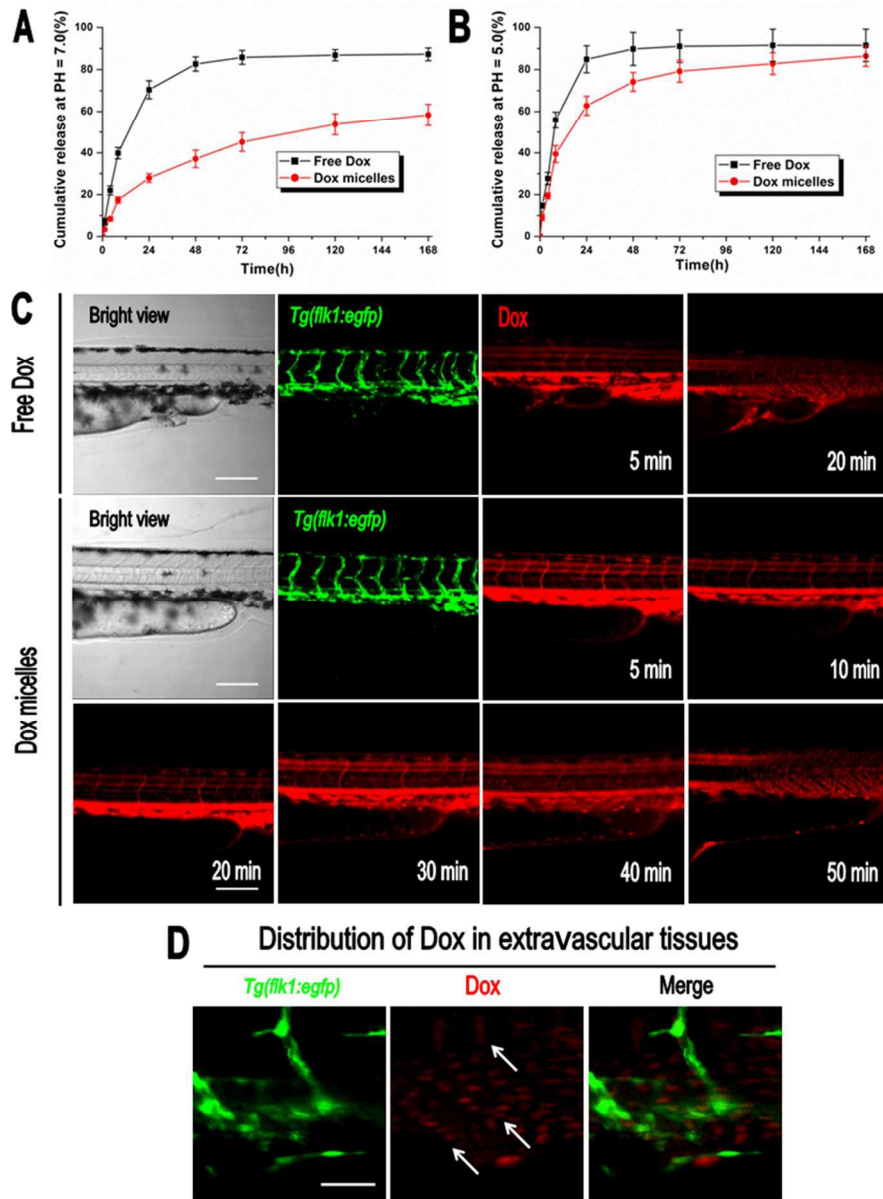
Preparation and characterization of Dox micelles. A: Appearance of free Dox (right) and Dox micelles (left) after centrifugation; B: Particle size distribution of Dox micelles; C: TEM image of Dox micelles. 84x60mm (300 x 300 DPI)



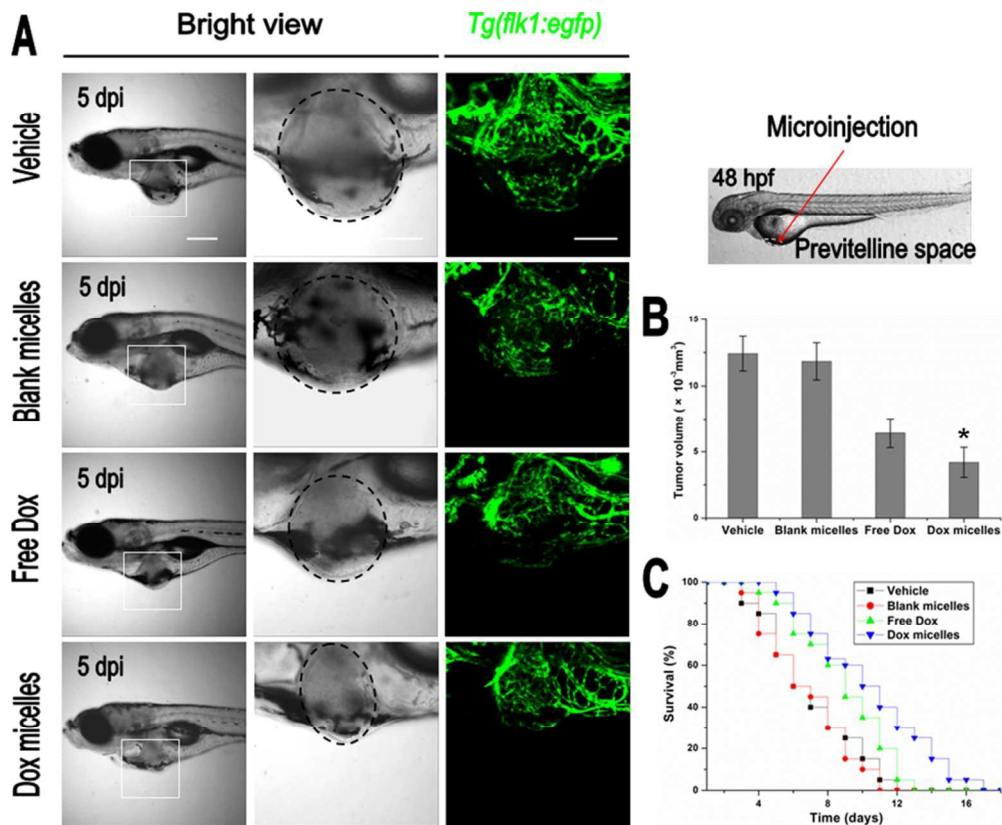
Cytotoxicity and apoptosis induction of Dox micelles. A: Cytotoxicity evaluation of blank micelles on 4T1 breast tumor cells; B: Cytotoxicity studies of free Dox and Dox micelles on 4T1 breast tumor cells; C: Images of 4T1 cells after 48 hours drug treatment, scale bar: 100  $\mu$ m; D: Apoptosis induction of Dox micelles and free Dox.  
84x58mm (300 x 300 DPI)



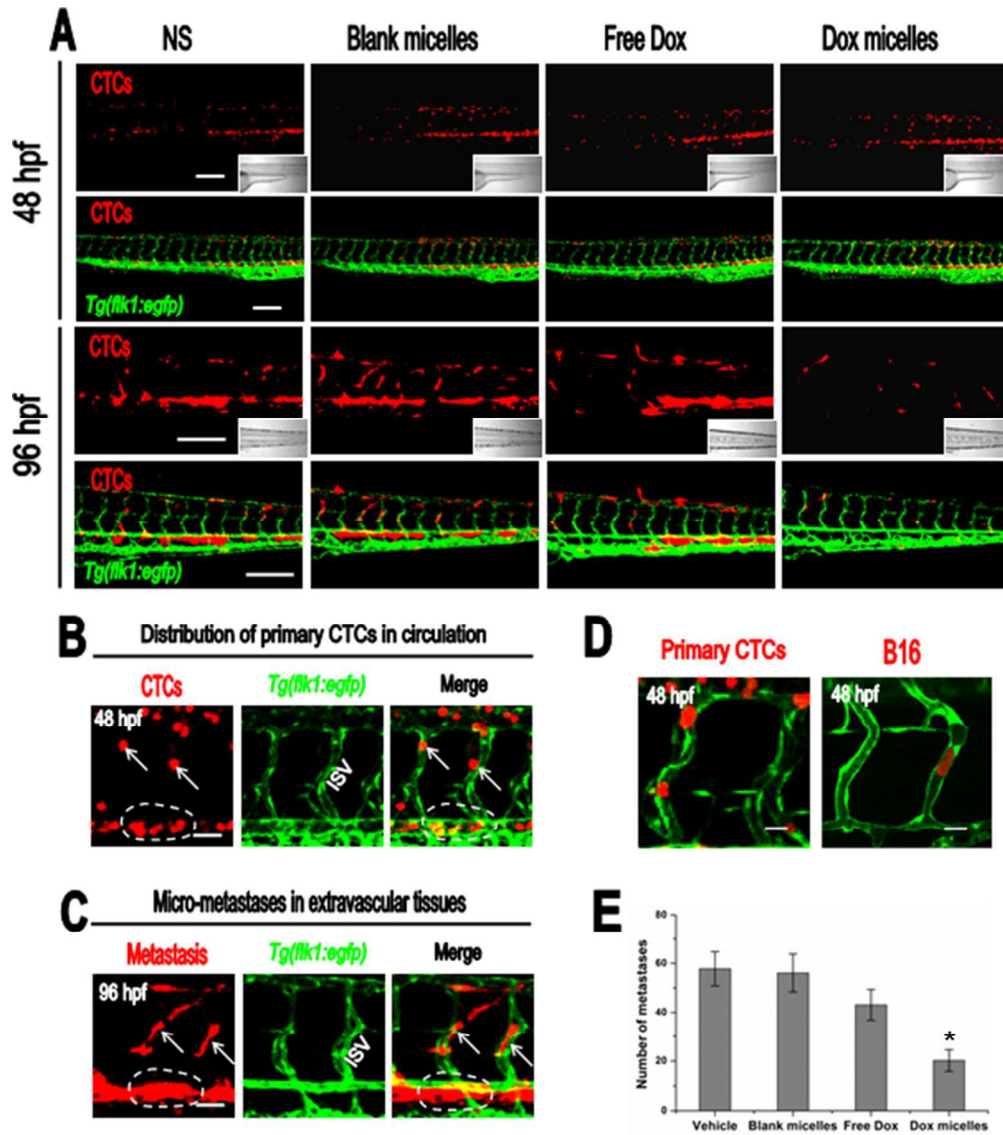
Cellular uptakes of Dox micelles and free Dox. A: Timelaps imaging the cellular uptake of Dox micelles and free Dox on 4T1 cells, red fluorescence indicates the cellular uptake of Dox while blue fluorescence indicates the cell nuclei which is staining by DAPI. Scale bar: 20  $\mu\text{m}$ ; B: Flow cytometric histograms for the Dox micelles on 4T1 cells; C: Dox accumulation in 4T1 cell by HPLC assay. 66x75mm (300 x 300 DPI)



In vitro release behavior and in vivo extravasation study of Dox micelles in Tg(flk1:egfp) transgenic zebrafish model. A and B: In vitro release behavior of Dox micelles and free Dox at pH 5.0 and pH 7.0, respectively; C: Dynamic extravasation behaviors of Dox micelles and free Dox in Tg(flk1:egfp) transgenic zebrafish model, scale bar: 150  $\mu$ m; D: Distribution of Dox in extravascular tissue, scale bar: 10  $\mu$ m. 84x115mm (300 x 300 DPI)

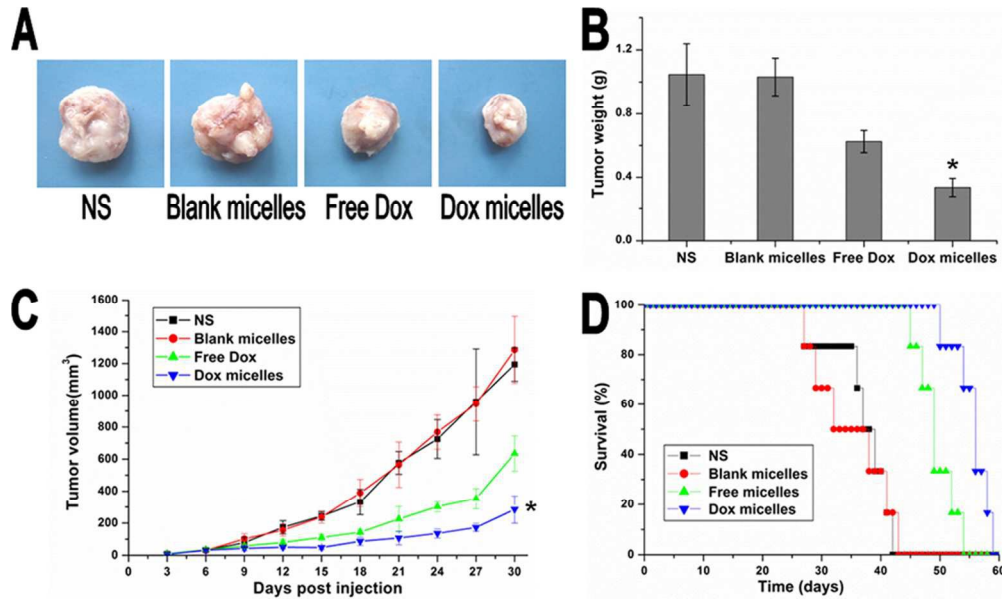


Anti-tumor studies of Dox micelles on *Tg(flk1:egfp)* transgenic zebrafish model. A: Images of anti-tumor effect in zebrafish 4T1 tumor model by Dox micelles and free Dox, scale bar: 200  $\mu\text{m}$ ; B: Tumor volume in each treatment group; C: Survival rate of zebrafish in each treatment group. 84x68mm (300 x 300 DPI)

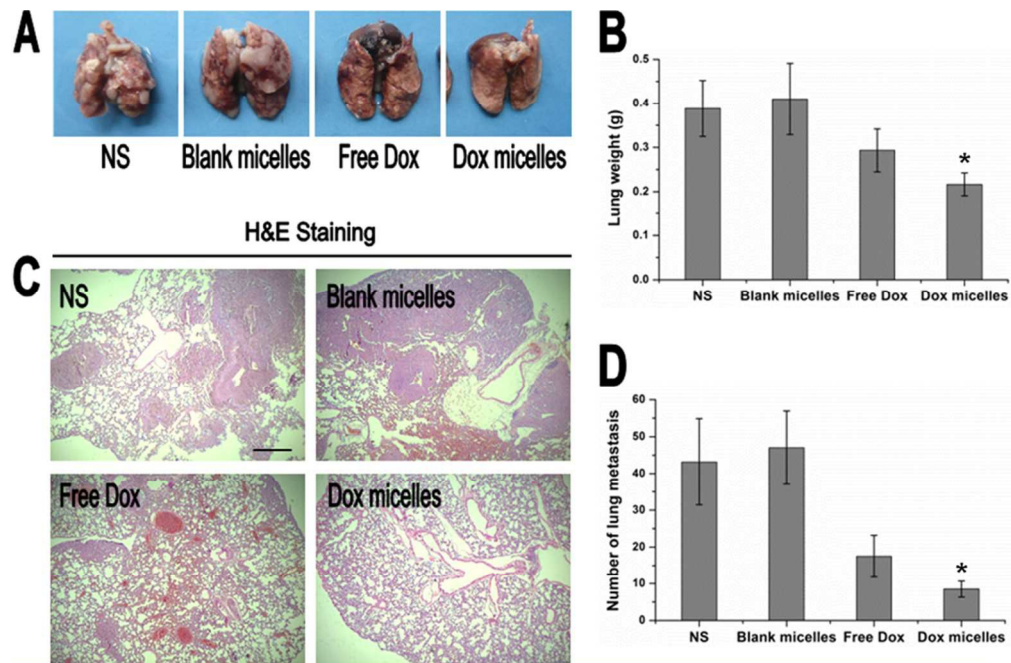


Anti-metastasis studies of Dox micelles in human primary CTCs injected Tg(flk1:egfp) transgenic zebrafish model. A: images of enhanced anti-metastasis effect of Dox micelles as contrasted to free Dox in human primary CTCs injected Tg(flk1:egfp) transgenic zebrafish model, scale bar: 100  $\mu$ m; B: Distribution of human primary CTCs in zebrafish blood vessels on 48 hpf, scale bar: 10  $\mu$ m; C: Distribution of micro-metastases in extravascular tissue on 96 hpf, scale bar: 10  $\mu$ m; D: Morphologic appearance of primary CTCs and B16 cell in zebrafish blood vessel, scale bar: 5  $\mu$ m; E: Number of micro-metastases in zebrafish extravascular tissue after 48 hours drug treatment.

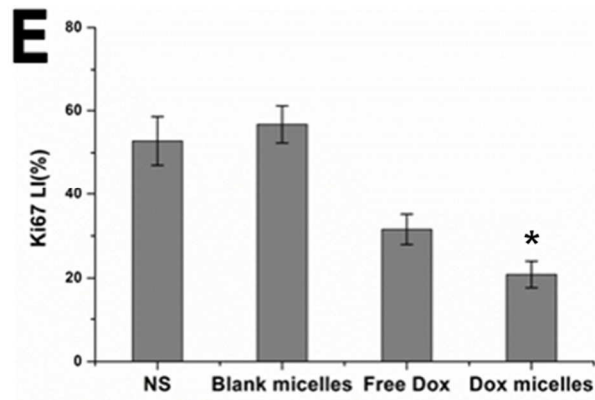
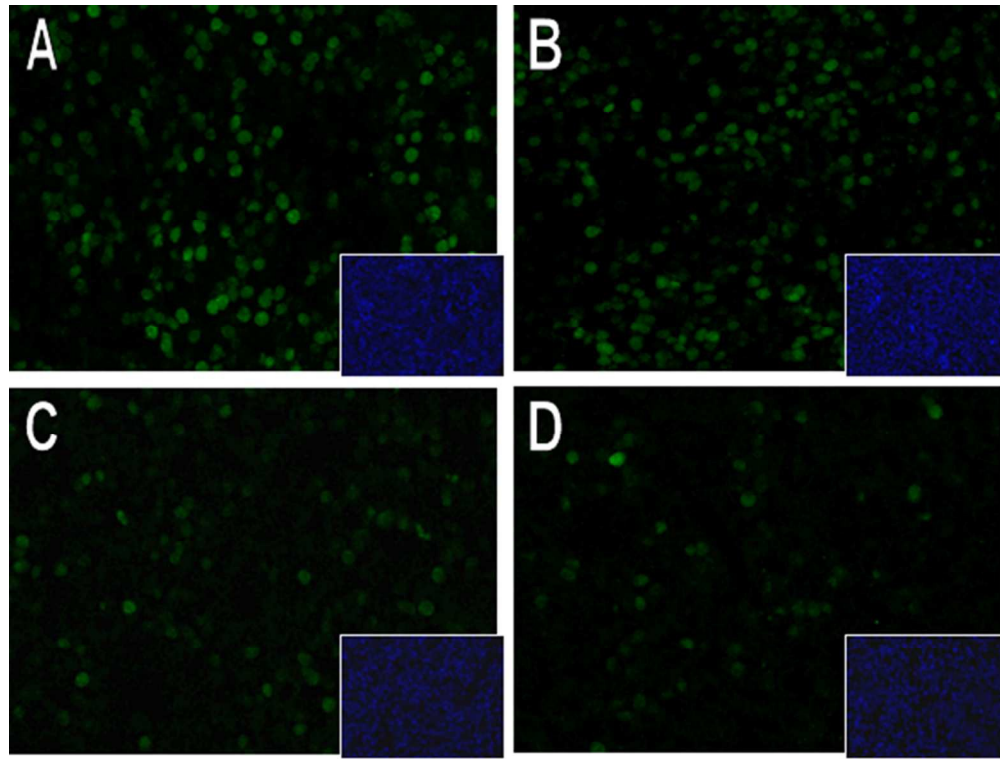
84x95mm (300 x 300 DPI)



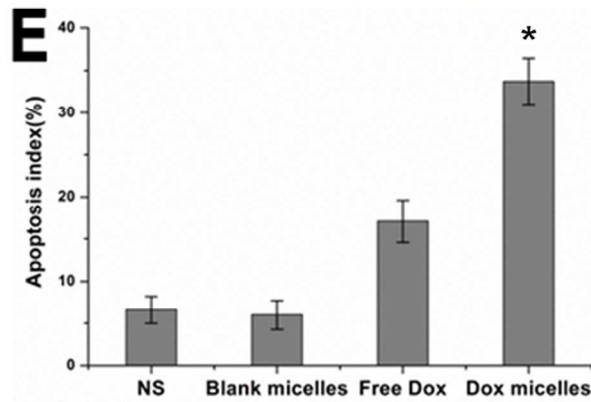
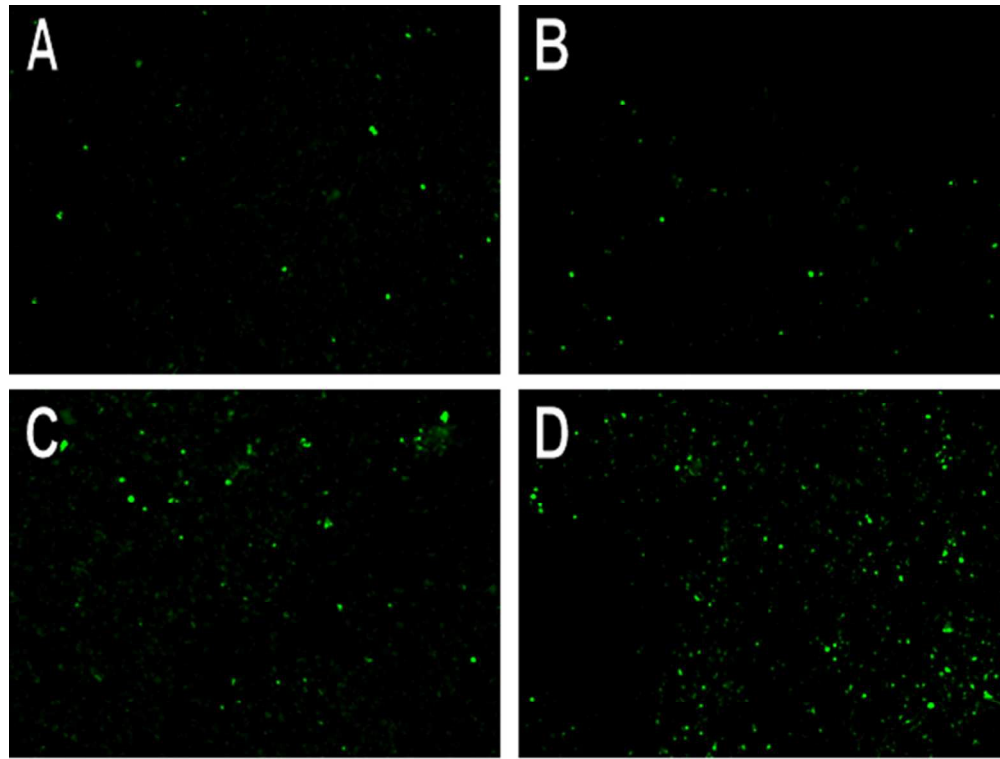
Dox micelles inhibit tumor growth in subcutaneous 4T1 model. A: Representative photographs of subcutaneous tumor in each treatment group; B: Tumor weight; C: Tumor volume; D: survival curve of mice in each group.  
84x50mm (300 x 300 DPI)



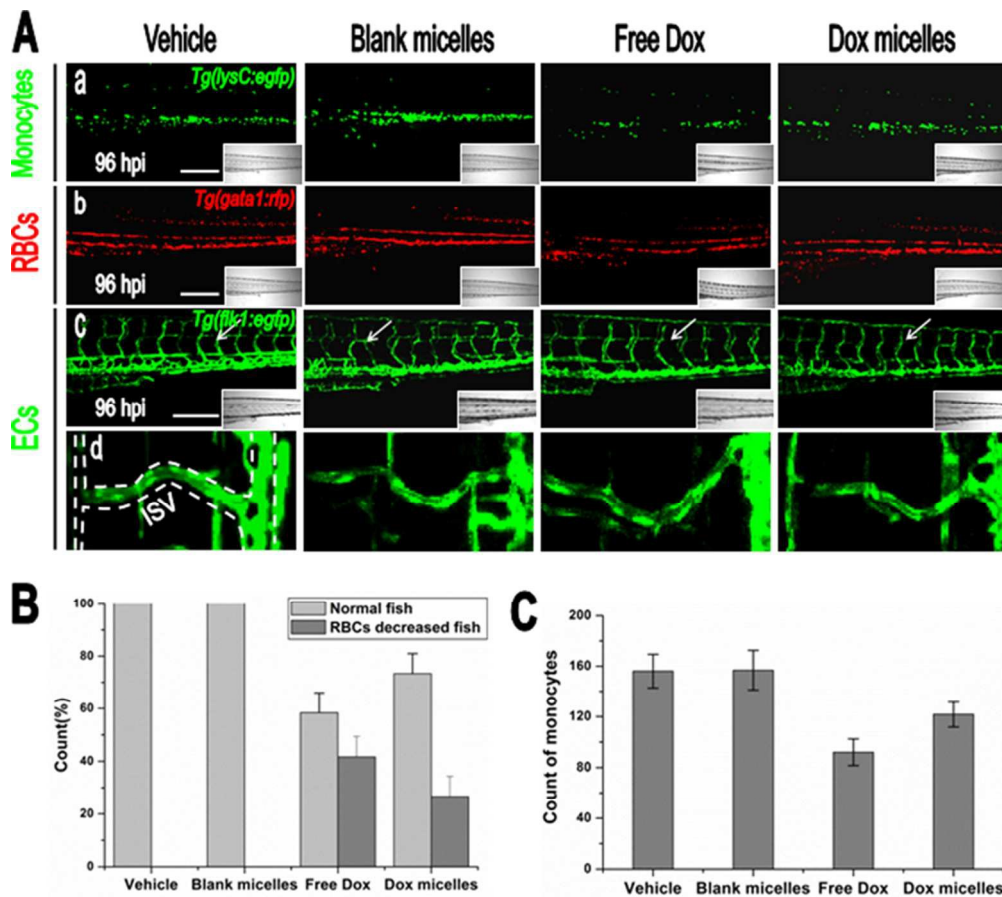
Dox micelles inhibit pulmonary metastasis in spontaneous metastatic 4T1 model. A: Representative photographs of pulmonary metastases in each group; B: Number of pulmonary metastases; C: HE staining of pulmonary section, scale bar: 400  $\mu$ m; D: Weight of lungs. 84x55mm (300 x 300 DPI)



Ki67 immunofluorescent staining of subcutaneous 4T1 tumor section, which suggested cell proliferation in subcutaneous 4T1 tumor. Representative Ki67 immunofluorescent images of NS (A), blank micelles (B), free Dox (C), and Dox micelles (D), and mean of Ki67 LI in each group (E).  
84x99mm (300 x 300 DPI)

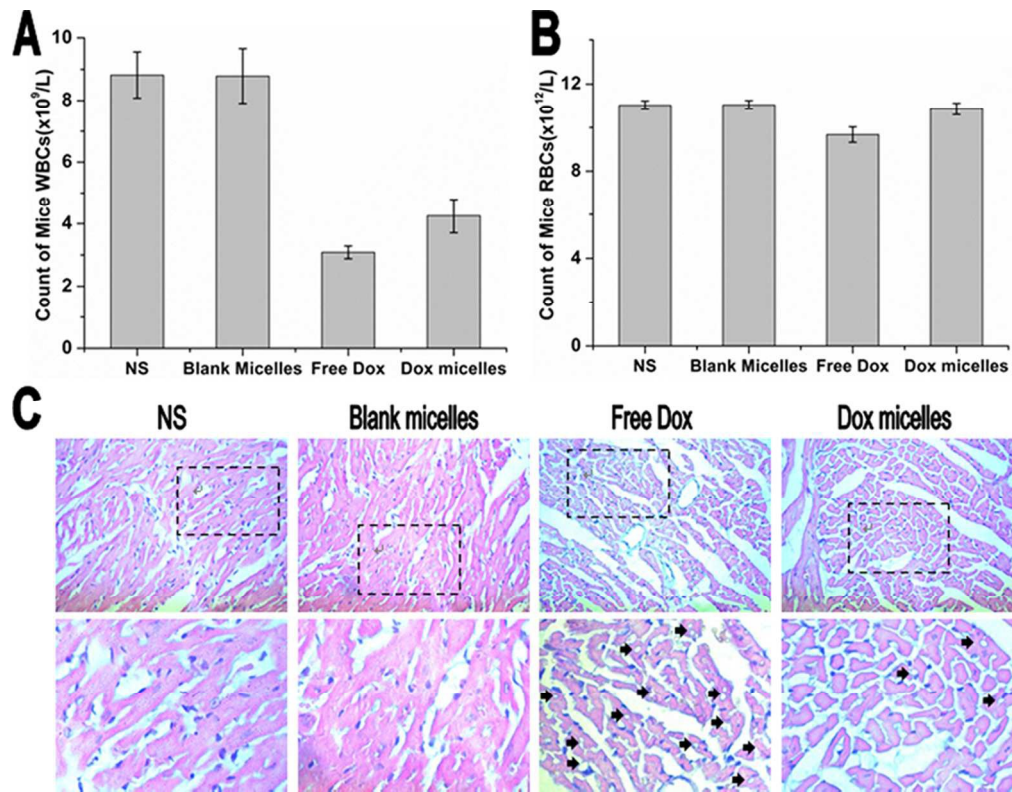


TUNEL immunofluorescent staining of subcutaneous 4T1 tumor section, which suggests cell apoptosis in subcutaneous 4T1 tumor. Representative TUNEL immunofluorescent images of NS (A), blank micelles (B), free Dox (C), and Dox micelles (D), and mean of apoptosis index in each group (E).  
84x100mm (300 x 300 DPI)



Toxicity evaluations of Dox micelles in transgenic zebrafish. A: Toxicity of Dox micelles to monocytes (a), RBCs (b) and ECs (c, d) in transgenic zebrafish model, scale bar: 100  $\mu$ m; B: Toxicity evaluation of Dox micelles to RBCs in Tg(flk1:egfp) zebrafish; C: Monocytes number of Tg(lysC:egfp) transgenic zebrafish in each treatment group.

84x75mm (300 x 300 DPI)



Toxicity evaluations of Dox micelles in mouse model. A: WBCs counting in each group; B: RBCs counting in each group; C: Cardiotoxicity evaluation of Dox micelles in mouse model. Black arrows showed the myocardial rupture holes  
84x66mm (300 x 300 DPI)